IEEE Access
Multidisciplinary | Rapid Review | Open Access Journal

Received July 6, 2018, accepted August 8, 2018, date of publication August 29, 2018, date of current version September 21, 2018.

Digital Object Identifier 10.1109/ACCESS.2018.2866329

Finite Memory Output Feedback Control for Unmanned Aerial Vehicle

HYUN HO KANG, SANG SU LEE, SUNG HYUN YOU, AND CHOON KI AHN, (Senior Member, IEEE)
School of Electrical Engineering, Korea University, Seoul 136-701, South Korea

Corresponding author: Choon Ki Ahn (hironaka@korea.ac.kr)

This work was supported in part by NRF through the Ministry of Science, ICT, and Future Planning under Grant NRF-2017R1A1A1A05001325 and in part by the Human Resources Program in Energy Technology of the Korea Institute of Energy Technology Evaluation and Planning Grant from the Ministry of Trade, Industry & Energy, South Korea, under Grant 20174030201820.

ABSTRACT In this paper, we propose a novel control strategy, a finite memory output feedback control (FMOFC), for an unmanned aerial vehicle (UAV). The proposed control strategy is designed with the estimated states obtained by stacking a finite N number of measurements, and the finite N number is defined as the horizon size, which represents the finite memory structure of the system. Through extending the concept of the horizon size by introducing a vector form to the augmented horizon size, the UAV is considered as a parallel system in terms of four independent states. Furthermore, the controller gain of the FMOFC is derived from the reconstructed parallel system under not only the finite memory structure, but also unbiasedness. Because of those constraints, the FMOFC exhibits a robust performance even in the presence of disturbance or unexpected noises from uncertainties, computational errors, and sudden changes in environments. The fast convergence and robust performance under disturbance or unexpected noises of the proposed control strategy are demonstrated through experimental results.

INDEX TERMS Finite memory structure, output feedback control, unbiasedness, robustness, unmanned aerial vehicle (UAV).

I. INTRODUCTION

Recently, research on unmanned aerial vehicles (UAVs) has become a more active and popular topic with the advent of the fourth industrial revolution. Because of the primary advantages of being able to fly in a desired or any direction and position, hover at any desired altitude, and take off and land vertically, UAVs are applied to several important applications such as managing agriculture [1], [2] rescues [3], [4], disaster or traffic monitoring [5], object detection [6]–[9], and mapping systems [8]–[10] extensively. However, UAVs have characteristics such as nonlinearity, uncertainties, and underactuation, so designing a robust controller for UAVs is not only challenging, but also an important issue [11]–[15].

Several studies propose control strategies for UAVs, and these can be classified in respect of the availability of states: state feedback control when all states are available [16], [17] and output feedback control when only partial states are available [18]–[22]. In [16], Yacef *et al.* presented the state feedback control strategy for the stabilization of a quadrotor UAV with the parallel disturbance compensation (PDC) technique, solving the linear matrix inequality (LMI) feasibility problem. In [17], Samir *et al.* proposed the state feedback control strategy with integral action to minimize steady-state errors for real-time trajectory-tracking problems.

However, due to the limitations in sensors and consideration of unexpected noises or disturbance in measurements, output feedback control strategies are considered more appropriate control strategies, and these are the major issues to be addressed intensively in this paper. The output feedback control strategies can be divided into two types in terms of control laws [18]–[22]: observer-based control and dynamic output feedback control. Observer-based output feedback control strategies are generally built with the state feedback control and an observer for estimating the unknown states with feedback gain. In [18], Islam *et al.* presented observer-based nonlinear adaptive output feedback control for miniature aerial vehicles with bounded uncertainty. They designed a model-free observer to estimate the linear and angular velocities of translational and rotational error dynamics with small constant proportional design parameters. In [19], Tognon *et al.* presented the observer-based control of the position and tension for an

aerial robot. They proposed the nonlinear control scheme considering the intrinsic characteristics of the aerial robot and high-gain observer based on a set of standard sensors to estimate unknown states and parameters. In [20], Dharmawan *et al.* proposed the linear quadratic regulator (LQR) and linear quadratic Gaussian (LQG) for the translation movement stability control of a quad tilt rotor, minimizing the linear quadratic (LQ) performance criterion. Dynamic output feedback control strategies are presented to compensate for various dynamical changes of UAVs through varying matrices in the state-space representation of modeling and control input. In [21], Wang and Han presented network-based modeling and dynamic output feedback control to provide much smaller oscillation amplitudes of the yaw velocity error and the yaw angle than the proportional-integral controller through the adoption of non-uniform distribution and the Wirtinger-based integral inequality approach. In [22], Dong and Hu presented time-varying dynamic output feedback control for linear multi-agent systems based on the separation principle through the generalized linear dynamics of N agents and determined the gain matrices by solving the Riccati equation.

Most existing output feedback control strategies for UAVs exhibit the infinite memory structure, which requires all the past measurements, where the linear quadratic Gaussian (LQG) control is a standard output feedback control with infinite memory structure [20], [23]–[25]. Because of the infinite memory structure of the existing output feedback controls, not only errors of noise information, but also uncertainties and round-off errors in computation can be accumulated for every time-step. The accumulation of these errors may lead to performance degradation and the divergence phenomenon in many cases. In other words, the existing output feedback controls have drawbacks in that they can be sensitive to the accumulation of noise information, uncertainties, and round-off errors in real-world environments. Therefore, there is high demand to design a controller to overcome the drawbacks of the existing output feedback controllers and to show robust performance even in the presence of these errors.

In this paper, we propose a novel output feedback control strategy, finite memory output feedback control (FMOFC), for a quadrotor UAV that can solve the above drawbacks. The FMOFC is designed under the finite memory structure, which satisfies the bounded input and bounded output (BIBO) stability and requires only the most recent N number of measurements, called the horizon. Because of the finite memory structure, the FMOFC can show robust performance, overcoming the addressed problems of existing controllers with the infinite memory structure and with less sensitivity to unexpected noises and uncertainties. The controller gain of the proposed strategy is determined to stabilize the error dynamics derived from the original state-space representation with states composed of velocities in the vehicle coordinate system and the yaw rate by defining a set of horizons corresponding to each state. Furthermore, the control inputs in the UAV are derived by obtaining auxiliary control inputs for the error dynamics. Through the experimental results, the robust performance of the FMOFC compared with the LQG control under the presence of disturbance signals or inaccurate noise information is demonstrated.

This paper consists of three sections. In Section 2, the state-space modeling of a UAV and the proposed output feedback control strategy, FMOFC, are presented. In Section 3, the experimental setup, and experimental results with trajectories of hovering, rectangular motion, and circular motion under disturbance signals are demonstrated. Finally, in Section 4, concluding remarks are presented.

II. FINITE MEMORY OUTPUT FEEDBACK CONTROL FOR UAV

In this section, the state-space modeling of a UAV and proposed control strategy, FMOFC, are discussed sequentially. Firstly, in the state-space modeling part, the state-space equations for designing the proposed control strategy are derived. Finally, the FMOFC is designed with the estimated state from the finite memory estimator.

A. STATE-SPACE MODELING

The coordinate system of the UAV can be divided into two types: the vehicle coordinate system (i.e., e_x^B, e_y^B, and e_z^B) and the inertial coordinate system (i.e., e_x^I, e_y^I, and e_z^I) as shown in Fig. 1. The relationship between the two coordinate systems can be represented by a rotational transformation matrix as follows [26]–[28]:

$$\dot{p} = Rv, \tag{1}$$

where

$$p = \begin{bmatrix} x & y & z \end{bmatrix}^T, \tag{2}$$

$$v = \begin{bmatrix} v_x & v_y & v_z \end{bmatrix}^T, \tag{3}$$

where p, v, and R represent the positions of the UAV in the inertial coordinate system, velocities of the UAV in the vehicle coordinate system, and rotational transformation matrix that converts from the vehicle coordinate system to the inertial

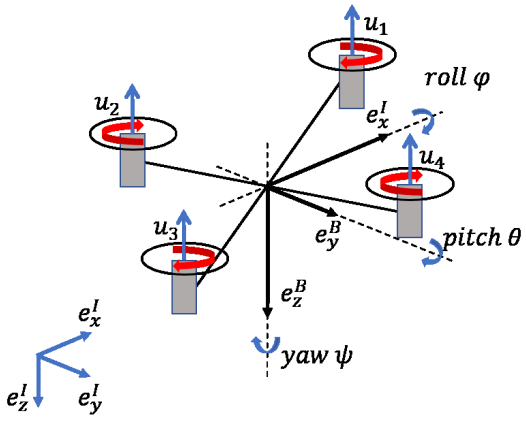

FIGURE 1. The inertial- and vehicle-coordinate systems of the UAV.

$$R = \begin{bmatrix} c(\theta)c(\psi) & s(\phi)s(\theta)c(\psi) - c(\phi)c(\psi) & c(\phi)s(\theta)c(\psi) + s(\phi)s(\psi) \\ c(\theta)s(\psi) & s(\phi)s(\theta)s(\psi) + c(\phi)c(\psi) & c(\phi)s(\theta)s(\psi) - s(\phi)c(\psi) \\ -s(\phi) & s(\phi)c(\theta) & c(\phi)c(\theta) \end{bmatrix}, \tag{4}$$

coordinate system, respectively. Each component of p and v, in (2)-(3), sequentially indicates the x-, y-, and z-positions and velocities, respectively. In (4), as shown at the top of this page, the cosine and sine functions are denoted by $c(\cdot)$ and $s(\cdot)$, and ϕ, θ, and ψ represent the roll, pitch, and yaw angles, respectively.

By defining u_1, u_2, u_3, u_4 as control inputs for the forces and torques generated by each propeller, the general dynamic model of the UAV with the outputs of the rotor signals can be written as follows [26]–[28]:

$$m\ddot{p} = u_1 \begin{bmatrix} c(\phi)s(\theta)c(\psi) + s(\phi)s(\psi) \\ c(\phi)s(\theta)s(\psi) - s(\phi)c(\psi) \\ c(\phi)c(\theta) \end{bmatrix} - mg \begin{bmatrix} 0 \\ 0 \\ 1 \end{bmatrix}, \tag{5}$$

$$\bar{I}\dot{w} + w \times (\bar{I}w) = \begin{bmatrix} u_2 \\ u_3 \\ u_4 \end{bmatrix}, \tag{6}$$

where

$$\bar{I} = \begin{bmatrix} I_{xx} & 0 & 0 \\ 0 & I_{yy} & 0 \\ 0 & 0 & I_{zz} \end{bmatrix},$$
$$w = \begin{bmatrix} w_x & w_y & w_z \end{bmatrix}^T.$$

In (5), m and g denote a mass of UAV and the gravitational acceleration, respectively. In (6), $\bar{I}$ denotes a system inertia matrix, where the inertia values in the x-, y-, and z-directions are arranged in a diagonal form and w represents a vector, considering the angular velocities in the x-, y-, and z-directions as components, sequentially.

By substituting the control inputs (i.e., u_1, u_2, u_3, u_4) into the x-, y-, and z-velocities and yaw rate, the state-space model of the UAV can be expressed as follows [26]–[28]:

$$\dot{V}_b = A_b V_b + B_b U_H, \tag{7}$$

where

$$V_b = \begin{bmatrix} v_x & v_y & v_z & \dot{\psi} \end{bmatrix}^T,$$
$$U_H = \begin{bmatrix} u_{v_x} & u_{v_y} & u_{v_z} & u_{\dot{\psi}} \end{bmatrix}^T,$$
$$A_b = -\begin{bmatrix} K_2 & 0 & 0 & 0 \\ 0 & K_4 & 0 & 0 \\ 0 & 0 & K_6 & 0 \\ 0 & 0 & 0 & K_8 \end{bmatrix}^T,$$
$$B_b = \begin{bmatrix} K_1 & 0 & 0 & 0 \\ 0 & K_3 & 0 & 0 \\ 0 & 0 & K_5 & 0 \\ 0 & 0 & 0 & K_7 \end{bmatrix}^T.$$

In (7), the state in the vehicle coordinate system and control input are denoted as V_b and U_H, respectively. U_H is the quantification of the combination of motor thrusts that generate the four dynamics of the UAV: longitudinal, lateral, vertical motion, and yawing. The corresponding motion and direction can be determined according to the magnitude and sign of the U_H value. $K_1, \cdots, K_8$, the diagonal components of A_b and B_b, are positive integers, and constants are obtained through system identification. In this paper, the state-space model of the UAV is obtained through the system identification based on the least squares method with input and output data from open loop experiment with AR Drone 2.0 [26]. The state-space model in the inertial coordinate system can be obtained by substituting the rotational transformation matrix, R, into (7) as follows:

$$\dot{V}_g = A_g V_g + B_g U_H, \tag{8}$$

where V_g represents the state in the inertial coordinate system. In (8), A_g and B_g can be obtained from following equations, respectively; $A_g = RA_bR^{-1}$ and $B_g = RB_b$. In this paper, since the controller is designed for roll and pitch angles as zero, a new rotational transformation matrix $\bar{R}$ is used instead of R and reformulated as follows:

$$\bar{R} \approx R,$$
$$= \begin{bmatrix} c(\psi) & -s(\psi) & 0 & 0 \\ s(\psi) & c(\psi) & 0 & 0 \\ 0 & 0 & 1 & 0 \\ 0 & 0 & 0 & 1 \end{bmatrix}.$$

B. FINITE MEMORY OUTPUT FEEDBACK CONTROL

The FMOFC considers a constant velocity (CV) model determining only positions and velocities by assuming accelerations and higher-order terms as noises. Therefore, the state with discrete-time index k can be defined as $x(k) = \begin{bmatrix} pos(k) & vel(k) \end{bmatrix}^T$, where $pos(k)$ and $vel(k)$ refer to the position and velocity, respectively. The state-space model in the discrete time can be written as follows:

$$x(k+1) = Ax(k) + w(k), \tag{9}$$
$$y(k) = Cx(k) + v(k), \tag{10}$$

where

$$A = \begin{bmatrix} 1 & \triangle t \\ 0 & 1 \end{bmatrix},$$
$$C = \begin{bmatrix} 1 & 0 \end{bmatrix},$$

where $x(k)$ and $\triangle t$ denote the state at time index k and the sampling period, respectively. $w(k)$ and $v(k)$ represent the process and measurement noises, respectively. They are assumed to be mutually uncorrelated and zero-mean white

Gaussian, and their covariances are defined as follows:

$$Q_w = \begin{bmatrix} q_1^2 & 0 \\ 0 & q_2^2 \end{bmatrix}, \quad R_v = r^2.$$

The augmented state of four number of independent states, $x_1(k)$, $x_2(k)$, $x_3(k)$, and $x_4(k)$ for the x, y, z, and yaw axes can be defined as follows:

$$X(k) = \left[x_1{}^T(k)\ x_2{}^T(k)\ x_3{}^T(k)\ x_4{}^T(k)\right]^T, \tag{11}$$

where

$$x_i(k) = \left[pos_i(k) \quad vel_i(k)\right]^T, \quad i = 1, 2, 3, 4.$$

The state-space model for augmented state $X(k)$ can be rewritten from (9)-(10) as follows:

$$X(k+1) = \bar{A}X(k) + W(k), \tag{12}$$
$$Y(k) = \bar{C}X(k) + V(k), \tag{13}$$

where

$$W(k) = \left[w_1{}^T(k) \quad w_2{}^T(k) \quad w_3{}^T(k) \quad w_4{}^T(k)\right]^T,$$
$$V(k) = \left[v_1(k) \quad v_2(k) \quad v_3(k) \quad v_4(k)\right]^T,$$
$$\bar{A} \triangleq I_4 \otimes A = \begin{bmatrix} A & 0 & 0 & 0 \\ 0 & A & 0 & 0 \\ 0 & 0 & A & 0 \\ 0 & 0 & 0 & A \end{bmatrix}, \tag{14}$$
$$\bar{C} \triangleq I_4 \otimes C = \begin{bmatrix} C & 0 & 0 & 0 \\ 0 & C & 0 & 0 \\ 0 & 0 & C & 0 \\ 0 & 0 & 0 & C \end{bmatrix}. \tag{15}$$

In (14)-(15), $\otimes$ denotes the Kronecker product of the matrices, where I_4 represents the 4×4 size of the identity matrix.

By defining the horizon size, which means the most recent number of measurements, corresponding to each state $x_i(k)$ as N_{x_i}, where $i = 1, 2, 3, 4$, the augmented horizon size $\mathbb{N}$ can be defined as follows:

$$\mathbb{N} = \left[N_{x_1} \quad N_{x_2} \quad N_{x_3} \quad N_{x_4}\right]. \tag{16}$$

From (16), a stacked-form matrix according to the exponent of matrix A and a new matrix $\mathbb{C}\{\mathbb{N}_j\}$ can be defined as follows:

$$\mathbb{C}\{\mathbb{N}_j\} = [I_{\mathbb{N}_j} \otimes C]\mathbb{A}\{\mathbb{N}_j - 1\}, \tag{17}$$

where

$$\mathbb{A}\{\mathbb{N}_j - 1\} = \begin{bmatrix} I \\ A \\ \vdots \\ A^{\mathbb{N}_j - 1} \end{bmatrix}, \tag{18}$$

where j denotes any positive integer that satisfies $j \leq 4$ and $\mathbb{N}_j$ is the jth element of $\mathbb{N}$. Generally, both $\mathbb{A}\{\cdot\}$ and $\mathbb{C}\{\cdot\}$, in (17)-(18), are the matrices that require a positive integer as an input; however in this paper, a positive integer is denoted as one of the elements of the augmented horizon size for convenience.

The maximum value among the elements of $\mathbb{N}$ can be defined as $\mathbb{N}_{max}$. For $k \geq \mathbb{N}_{max}$, the batch form of (12)-(13) on the horizons $[k - \mathbb{N}_j, k - 1]$, where $j = 1, 2, 3, 4$, can be obtained as follows:

$$X(k) = \bar{A}^{\mathbb{N}_j}X(k - \mathbb{N}_j) + M_{\mathbb{N}_j}\Pi(k-1), \tag{19}$$
$$\bar{Y}(k-1) = \bar{C}_{\mathbb{N}_j}X(k - \mathbb{N}_j) + mG_{\mathbb{N}_j}\Pi(k-1) + \Omega(k-1), \tag{20}$$

where

$$\bar{A}^{\mathbb{N}_j} \triangleq \begin{bmatrix} A^{\mathbb{N}_1} & 0 & 0 & 0 \\ 0 & A^{\mathbb{N}_2} & 0 & 0 \\ 0 & 0 & A^{\mathbb{N}_3} & 0 \\ 0 & 0 & 0 & A^{\mathbb{N}_4} \end{bmatrix},$$
$$M_{\mathbb{N}_j} \triangleq \left[\bar{A}^{\mathbb{N}_j - 1} \quad \bar{A}^{\mathbb{N}_j - 2} \quad \cdots \quad I_8\right],$$
$$\Pi(k-1) \triangleq \left[W^T(k-\mathbb{N}_j) \quad W^T(k-\mathbb{N}_j+1) \quad \cdots \quad W^T(k-1)\right]^T,$$
$$\bar{Y}(k-1) \triangleq \left[y_1(k-\mathbb{N}_1)\cdots y_1(k-1) \quad \cdots \quad y_4(k-\mathbb{N}_4)\cdots y_4(k-1)\right]^T,$$
$$\Omega(k-1) \triangleq \left[V^T(k-\mathbb{N}_j)\ V^T(k-\mathbb{N}_j+1) \cdots V^T(k-1)\right]^T,$$
$$\bar{C}_{\mathbb{N}_j} = \begin{bmatrix} \mathbb{C}\{\mathbb{N}_1\} & 0 & 0 & 0 \\ 0 & \mathbb{C}\{\mathbb{N}_2\} & 0 & 0 \\ 0 & 0 & \mathbb{C}\{\mathbb{N}_3\} & 0 \\ 0 & \cdots & 0 & \mathbb{C}\{\mathbb{N}_4\} \end{bmatrix},$$
$$= \begin{bmatrix} 1 & 0 & 0 & \cdots & 0 \\ 1 & \triangle t & 0 & \cdots & 0 \\ \vdots & \vdots & \vdots & \cdots & \\ 1 & (\mathbb{N}_1 - 1)\triangle t & 0 & & 0 \\ 0 & 0 & & & \\ & & \ddots & & \vdots \\ \vdots & \vdots & & 0 & 0 \\ & & \ddots & 1 & 0 \\ & & & 1 & \triangle t \\ & & & \vdots & \vdots \\ 0 & 0 & 0 & 1 & (\mathbb{N}_4 - 1)\triangle t \end{bmatrix},$$
$$L = \begin{bmatrix} 0 & 0 & 0 \\ \mathbb{C}\{\mathbb{N}_1 - 1\} & 0 & \vdots \\ 0 & 0 & \\ & \mathbb{C}\{\mathbb{N}_2 - 1\} & \\ \vdots & 0 & 0 \\ & \vdots & \mathbb{C}\{\mathbb{N}_3 - 1\} \\ & & 0 \\ 0 & 0 & 0 \end{bmatrix}$$
$$\begin{bmatrix} 0 & 0 & \cdots & 0 \\ & \mathbb{C}\{\mathbb{N}_1 - 2\} & & \\ & 0 & \ddots & \vdots \\ \vdots & & & 0 \\ & \vdots & \ddots & \\ & & & \vdots \\ 0 & & & \\ \mathbb{C}\{\mathbb{N}_4 - 1\} & 0 & \cdots & 0 \end{bmatrix}.$$

(19)-(20) can be rewritten by taking the expectation as follows:

$$E[X(k)] = \bar{A}^{\mathbb{N}_j} E[X(k-\mathbb{N}_j)], \tag{21}$$

$$E[\bar{Y}(k-1)] = \bar{C}_{\mathbb{N}_j} E[X(k-\mathbb{N}_j)]. \tag{22}$$

The finite memory estimator can be designed as follows:

$$\hat{X}(k) = \mathcal{H}\bar{Y}(k-1), \tag{23}$$

where $\hat{X}(k)$ and $\mathcal{H}$ represent the estimated state and gain matrix of the finite memory estimator, respectively. By combining the expectation result of (23) with (22), the finite memory estimator can be rewritten as follows:

$$E[\hat{X}(k)] = \mathcal{H}\bar{C}_{\mathbb{N}_j}\bar{A}^{-\mathbb{N}_j} E[X(k)]. \tag{24}$$

From the unbiasedness condition, $E[\hat{X}(k)] = E[X(k)]$, and a variable substitution, $\bar{C}_O = \bar{C}_{\mathbb{N}_j}\bar{A}^{-\mathbb{N}_j}$, (24) can be represented as follows:

$$\mathcal{H}\bar{C}_O = I, \tag{25}$$

where

$$\bar{C}_O = \begin{bmatrix} 1 & -\mathbb{N}_1\triangle t & 0 & & \cdots & & 0 \\ & & & & \cdots & & 0 \\ \vdots & \vdots & \vdots & & & & \vdots \\ 1 & -\triangle t & 0 & & \cdots & & 0 \\ 0 & 0 & 1 & -\mathbb{N}_2\triangle t & & & \\ & & & & \ddots & & \vdots \\ & & \vdots & \vdots & & & \\ \vdots & \vdots & 1 & -\triangle t & & 0 & 0 \\ & & 0 & 0 & \ddots & 1 & -\mathbb{N}_4\triangle t \\ & & \vdots & \vdots & & & \\ & & & & & \vdots & \vdots \\ 0 & 0 & \cdots & & 0 & 1 & -\triangle t \end{bmatrix}. \tag{26}$$

Through (24), it can be confirmed that (26) represents the observability matrix. For the two conditions, non-zero $\triangle t$ and $\mathbb{N}_j \geq 2$, where $j = 1, 2, 3, 4$, (26) shows the full rank property. Therefore, each element of $\mathbb{N}$ can be any positive integer that is greater than or equal to 2.

From (23) and (25), the gain matrix $\mathcal{H}$ can be represented as follows:

$$\mathcal{H} = \begin{bmatrix} \hbar_{(1,1)} & \hbar_{(1,2)} & \cdots & \hbar_{(1,\mathbb{N}_{total})} \\ \hbar_{(2,1)} & \hbar_{(2,2)} & \cdots & \hbar_{(2,\mathbb{N}_{total})} \\ \hbar_{(3,1)} & \hbar_{(3,2)} & \cdots & \hbar_{(3,\mathbb{N}_{total})} \\ \hbar_{(4,1)} & \hbar_{(4,2)} & \cdots & \hbar_{(4,\mathbb{N}_{total})} \end{bmatrix}, \tag{27}$$

where

$$\hbar_{(m,n)} = \begin{bmatrix} \alpha_{(m,n)} & \beta_{(m,n)} \end{bmatrix}^T, \tag{28}$$

$$\mathbb{N}_{total} = \sum_{j=1}^{4} \mathbb{N}_j, \tag{29}$$

with $m = 1, 2, 3, 4$. In (27), $\hbar_{(m,n)}$ and $\mathbb{N}_{total}$ represent the mth row and nth column element of the gain matrix related to the mth state of $X(k)$, and the sum of all elements of the augmented horizon size, respectively. From (25)-(27), it is noted that $\hbar_{(m,n)}$ is not zeros only for $\sum_{j=1}^{m-1}\mathbb{N}_j < n \leq \sum_{j=1}^{m}\mathbb{N}_j$. For example, if m is assumed to be 1, $\hbar_{(1,\mathbb{N}_1+1)}, \cdots, \hbar_{(1,\mathbb{N}_{total})}$ are all zeros and the remaining parts, $\hbar_{(1,1)}, \cdots, \hbar_{(1,\mathbb{N}_1)}$, have specific integers related to the mth state. Therefore, by combining (25) and (27), the conditions can be derived as follows:

$$\sum_{n=1}^{\mathbb{N}_m} \hbar_{(m,n+\kappa_m)} = \begin{bmatrix} 1 & 0 \end{bmatrix}^T, \tag{30}$$

$$\triangle t \sum_{n=1}^{\mathbb{N}_m} (-\mathbb{N}_m - 1 + n)\hbar_{(m,n+\kappa_m)} = \begin{bmatrix} 0 & 1 \end{bmatrix}^T, \tag{31}$$

where

$$\kappa_i = \sum_{k=j}^{i-1} \mathbb{N}_j. \tag{32}$$

Considering (25), there are numerous solutions for the gain matrix; however, under the constraints (30)-(31), the solution for (25) can be obtained by minimizing the following cost function; $J_\hbar = \sum_{n=1}^{\mathbb{N}_m} \hbar_{(m,n+\kappa_m)}^T \hbar_{(m,n+\kappa_m)}$. The Lagrange function, one of the methods to obtain $\hbar_{(m,n+\kappa_m)}$ that minimizes the cost function $J_\hbar$, is introduced, and the Lagrange function can be written as follows:

$$\begin{aligned} \mathcal{L} = &\sum_{n=1}^{\mathbb{N}_m} \hbar_{(m,n+\kappa_m)}^2 + \lambda_1 (1 - \sum_{n=1}^{\mathbb{N}_m} \hbar_{(m,n+\kappa_m)}) \\ &+ \lambda_2 \sum_{n=1}^{\mathbb{N}_m} (-\mathbb{N}_m - 1 + n)\hbar_{(m,n+\kappa_m)} \triangle t, \end{aligned} \tag{33}$$

where both λ_1 and λ_2 are Lagrange multiplier vectors. By taking a partial derivative of the Lagrange function with respect to $\hbar_{(m,n+\kappa_m)}$, (33) can be rewritten as follows:

$$\frac{\partial \mathcal{L}}{\partial \hbar_{(m,n+\kappa_m)}} = 2\hbar_{(m,n+\kappa_m)} - \lambda_1 + \lambda_2(\mathbb{N}_m + 1 - n)\triangle t. \tag{34}$$

Making (34) zero, $\hbar_{(m,n+\kappa_m)}$ can be obtained as follows:

$$\hbar_{(m,n+\kappa_m)} = \frac{\lambda_1 - \lambda_2(\mathbb{N}_m + 1 - n)\triangle t}{2}. \tag{35}$$

By substituting (35) into (30)-(31), $\hbar_{(m,n+\kappa_m)}$ can be rewritten as follows:

$$\hbar_{(m,n+\kappa_m)} = \begin{bmatrix} \dfrac{-2\mathbb{N}_m + 6n - 4}{\mathbb{N}_m(\mathbb{N}_m - 1)} \\ \dfrac{-6\mathbb{N}_m + 12n - 6}{\mathbb{N}_m(\mathbb{N}_m - 1)(\mathbb{N}_m + 1)} \end{bmatrix}, \tag{36}$$

with $n = 1, \cdots, \mathbb{N}_m$. The gain matrix $\mathcal{H}$ of the finite memory estimator can be obtained by the Lagrange function as

follows:

$$\mathcal{H} = \begin{bmatrix} \mathcal{H}_{\mathbb{N}_1} & 0 & 0 & 0 \\ 0 & \mathcal{H}_{\mathbb{N}_2} & 0 & 0 \\ 0 & 0 & \mathcal{H}_{\mathbb{N}_3} & 0 \\ 0 & 0 & 0 & \mathcal{H}_{\mathbb{N}_4} \end{bmatrix}, \tag{37}$$

where

$$\mathcal{H}_{\mathbb{N}_i} = \left[\hbar_{(i,1)}\ \hbar_{(i,2)} \cdots \hbar_{(i,\mathbb{N}_m)}\right], \quad i = 1, 2, 3, 4,$$

where $\mathcal{H}_{\mathbb{N}_i}$ denotes the gain matrix of the ith state $x_i(k)$. The final structure of the gain matrix $\mathcal{H}$ is composed of the gain matrices of each independent state. The gain matrix of the finite memory estimator can be designed as one large matrix from the augmented state. Therefore, the gain matrices obtained from the augmented state and the four independent states are in a parallel relationship with each other.

The controller is designed to minimize error terms between the velocities of the UAV and the reference velocities. Because the velocities of the UAV are inaccessible states and the measurements are vulnerable to disturbance or inaccurate noise information, the estimated velocities from the finite memory estimator are considered the velocities of the UAV. In other words, the FMOFC is designed to obtain control inputs that minimize the error terms of the estimated and reference velocities. The discretization of (7) can be performed as follows:

$$V_b(k+1) = \hat{A}_b V_b(k) + \hat{B}_b U_H(k), \tag{38}$$

where

$$\hat{A}_b = I + A_b,$$
$$\hat{B}_b = B_b \triangle t,$$

where $V_b(k)$ and $U_H(k)$ represent the state and control input at time step k.

In (38), $V_b(k)$ can be substituted into the estimated state $\hat{V}_b(k)$ through (23) and by defining a reference value of $V_b(k)$ as $V_{b,ref}(k)$, (38) can be rewritten as follows:

$$\begin{aligned} V_{b,ref}(k+1) - \hat{V}_b(k+1) &= \hat{A}_b(V_{b,ref}(k) - \hat{V}_b(k)) - \hat{A}_b V_{b,ref}(k) \\ &\quad - \hat{B}_b U_H(k) + V_{b,ref}(k+1), \end{aligned} \tag{39}$$

where

$$\hat{V}_b(k) = I_4 \otimes \begin{bmatrix} 0 & 0 \\ 0 & 1 \end{bmatrix} \mathcal{H} Y_b(k-1),$$

where $\hat{V}_b(k)$ and $Y_b(k-1)$ represent the estimated velocities and stacked measurements of the UAV during the horizons, respectively.

By defining the error term as $\tilde{V}_b(k) = V_{b,ref}(k) - \hat{V}_b(k)$, (39) can be reformulated as follows:

$$\begin{aligned} \tilde{V}_b(k+1) = \hat{A}_b \tilde{V}_b(k) - \hat{B}_b[U_H(k) \\ + \hat{B}_b^{-1}(\hat{A}_b V_{b,ref}(k) - V_{b,ref}(k+1))]. \end{aligned} \tag{40}$$

From (40), a new system in terms of the error term can be designed through a new control input defined as $\tilde{U}_H(k) = -U_H(k) - \hat{B}_b^{-1}(\hat{A}_b V_{b,ref}(k) - V_{b,ref}(k+1))$ as follows:

$$\tilde{V}_b(k+1) = \hat{A}_b \tilde{V}_b(k) + \hat{B}_b \tilde{U}_H(k). \tag{41}$$

The cost function is considered as follows:

$$J = \sum_{k=0}^{\infty} \tilde{V}_b^T(k) \bar{Q} \tilde{V}_b(k) + \tilde{U}_H^T(k) \bar{P} \tilde{U}_H(k), \tag{42}$$

where $\bar{Q}$ and $\bar{P}$ are diagonal matrices and design parameters that can improve the convergence performance of the ith state. The control law to minimize the cost function is expressed as follows:

$$\tilde{U}_H(k) = -K \tilde{V}_b(k), \tag{43}$$

where K represents a controller gain. Therefore, (41) can be rewritten in a closed loop system by substituting the control law (43) into (41) as follows:

$$\tilde{V}_b(k+1) = (\hat{A}_b - \hat{B}_b K) \tilde{V}_b(k), \tag{44}$$

where the K should be designed to make the eigenvalues of $(\hat{A}_b - \hat{B}_b K)$ have a negative real part: the Hurwitz matrix. The controller gain K can be calculated from the equation as follows:

$$K = (\bar{P} + \hat{B}^T \tilde{P} \hat{B})^{-1} (\hat{B}^T \tilde{P} \hat{A}), \tag{45}$$

where $\tilde{P}$ is the unique positive definite solution of the Riccati equation [29], [30]. From (45), the control input $U_H(k)$ of the original system (38) can be reformulated as follows:

$$\begin{aligned} U_H(k) = K(V_{b,ref}(k) - \hat{V}_b(k)) \\ - \hat{B}_b^{-1}(\hat{A}_b V_{b,ref}(k) - V_{b,ref}(k+1)). \end{aligned} \tag{46}$$

The block diagram of the proposed control strategy, FMOFC, can be seen in Fig. 2. The estimated state $\hat{V}_b(k)$ can be obtained by stacking the augmented measurement of the x-, y-, and z-positions and yaw angle up to the augmented horizon size, as shown in (23). Furthermore, the controller is designed to minimize the error term $\tilde{V}_b(k)$ between the estimated state and reference value, as shown in (42). Finally, the control input is calculated and generated from the FMOFC which is formulated in (46).

III. EXPERIMENT

This section is divided into two subsections: the experimental setup and experimental results. One covers the experimental equipment in detail and explains the experimental goals. The other shows the experimental results to demonstrate the robust performance of the proposed control strategy, FMOFC.

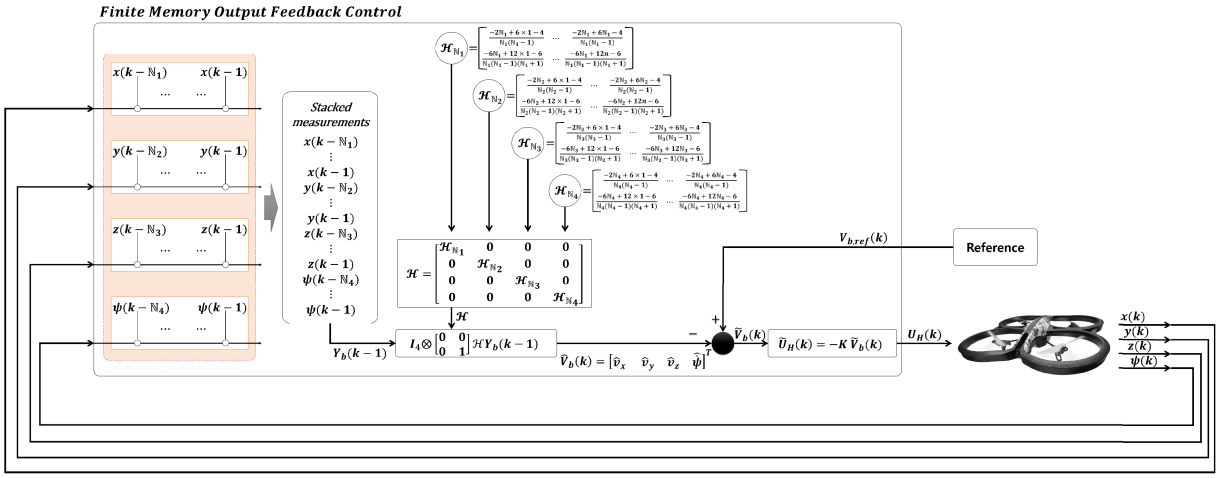

FIGURE 2. Block diagram of finite memory output feedback control.

A. EXPERIMENTAL SETUP

The experiments were conducted through MATLAB to maintain three kinds of given paths in the presence of disturbance: hovering, rectangular motion, and circular motion experiments. For the experiments, the following equipment was used; a computer, a Local Area Network (LAN) card, and an AR. Drone 2.0. The computer for the ground station communicated with the drone to send control inputs or receive sensor data. Intel(R) Core(TM) i7-7700 CPU@3.60Hz and 16.0GB were used for the processor and RAM of the ground station, respectively. The system type was a 64-bit operating system. The LAN card was used to improve communication between the ground station and drone. The NEXT-1200AC was used for the LAN card, which complied with the IEEE 802.11ac, IEEE 802.11a, IEEE 802.11n, IEEE 802.11g, and IEEE 802.11b standards and provided a USB 3.0 port. Furthermore, it provided a 300/867Mbps receiving rate and 300/867Mbps sending rate.

B. EXPERIMENTAL RESULTS

In this section, the four performed experiments are introduced: the determination of the augmented horizon size of the finite memory estimator, hovering, rectangular motion, and circular motion experiments. Through the experimental results, the robust performance of the proposed control strategy is demonstrated in the case of unexpected disturbance.

1) DETERMINATION OF HORIZON SIZES

The proper augmented horizon size of the finite memory estimator was obtained from the minimum value of the root mean square errors (RMSEs) defined for each of the four independent states as follows:

$$J_{\mathbb{N}_i} = \sqrt{\sum_{k=t_{init}}^{t_{final}} (\hat{x}_i(k) - x_{i,ref}(k))^2}, \tag{47}$$

where

$$\mathbb{N} = \begin{bmatrix} N_{x_1} & N_{x_2} & N_{x_3} & N_{x_4} \end{bmatrix},$$

with $i = 1, 2, 3, 4$ for the x-, y-, and z- velocities and yaw rate. In (47), t_{init} is the initial time of the experiment and t_{final} is the final time of the experiment, which were set to zero and 100 seconds, respectively, and the RMSEs were obtained from the results during 100 seconds, a difference between t_{init} and t_{final}. $\hat{x}_i(k)$ and $x_{i,ref}(k)$ represent the value of the ith current estimated state of the UAV and reference state at time k, respectively. In addition, the term $\hat{x}_i(k) - x_{i,ref}(k)$ represent the errors between the ith estimated state and the reference state. The proper horizon size for each ith state can be obtained at the minimum value of the RMSEs with the Monte Carlo method, and the results are shown in Fig. 3: (a), (b), (c), and (d).

As shown in Fig. 3, the graphs of the RMSEs over various horizon sizes are represented in a convex form and show minimum values at the horizon sizes 4, 3, 4, and 4, respectively, for each independent state. Consequently $\mathbb{N}$ can be obtained as follows:

$$\mathbb{N} = \begin{bmatrix} 4 & 3 & 4 & 4 \end{bmatrix}.$$

2) HOVERING EXPERIMENT

In the hovering experiment, the reference values were set for the drone to hover at a height of 1 meter. A sine curve with an amplitude of 0.1 meters and an impulse with a value of 0.1 meters were injected overall in the hovering experiment as disturbance signals.

The hovering results of the UAV are indicated in a three-dimensional coordinate system, as shown in Fig. 4: (a) LQG control and (b) the proposed control strategy, FMOFC. In Fig. 4(a), the LQG control eventually returns to the original hovering position; however, it shows large amounts of overshoot. When the disturbance signals were injected, the LQG control shows that the x or y positions reached the point with a

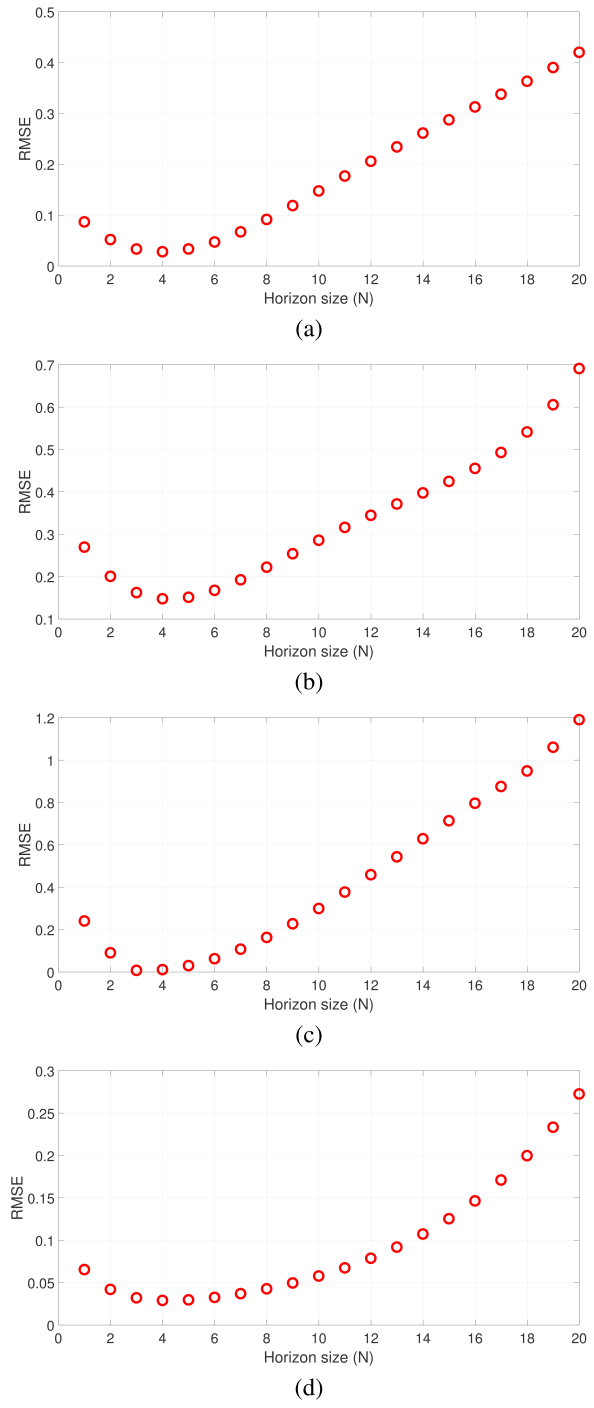

FIGURE 3. RMSEs for various horizon sizes: (a) x velocity, (b) y velocity, (c) z velocity, and (d) yaw rate.

value of 0.1. On the other hand, the proposed method returned to the original position with smaller amounts of overshoot than the LQG control, as shown in Fig. 4(b). The results can be more clearly seen in Table 1, the RMSE comparison table in terms of the x and y positions. As shown in Table 1, the RMSE value of the proposed control strategy is approximately four times lower than the LQG control strategy both

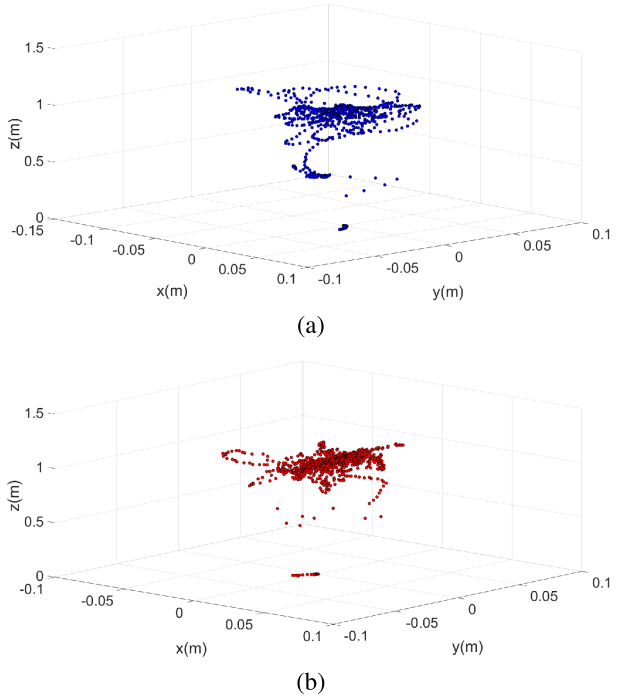

FIGURE 4. Hovering experiment results in 3-dimensional coordinate system: (a) LQG control and (b) FMOFC (proposed).

TABLE 1. RMSE comparison in hovering experiment.

	LQG control	FMOFC (proposed)
x position	0.3408	0.0813
y position	0.4721	0.1028

in the x and y positions. As a result, the FMOFC shows a robust performance against the disturbance in the hovering experiment.

3) RECTANGULAR MOTION EXPERIMENT

In the rectangular motion experiment, the reference values were set to move the drone in the shape of a square with a length of 1 meter on each side while maintaining a height of 1 meter. Impulse signals with a value of 0.3 meters were injected as disturbance signals when the UAV reached each corner of the square.

The experimental results of the UAV are indicated in a three-dimensional coordinate system as shown in Fig. 5: (a) LQG control and (b) the proposed control strategy, FMOFC. From Fig. 5(a), even in the case of disturbance, the UAV with LQG control returned to the original position at each corner of a given path. However, significant amounts of overshoot occur when the signals with a value of 0.3 meters were injected as disturbance signals, so that it nearly reached the position of 1.5 meters in both the x and y positions. In the end, the LQG control showed the divergence phenomenon without returning to the initial position due to the accumulation of errors and unexpected disturbance. On the other

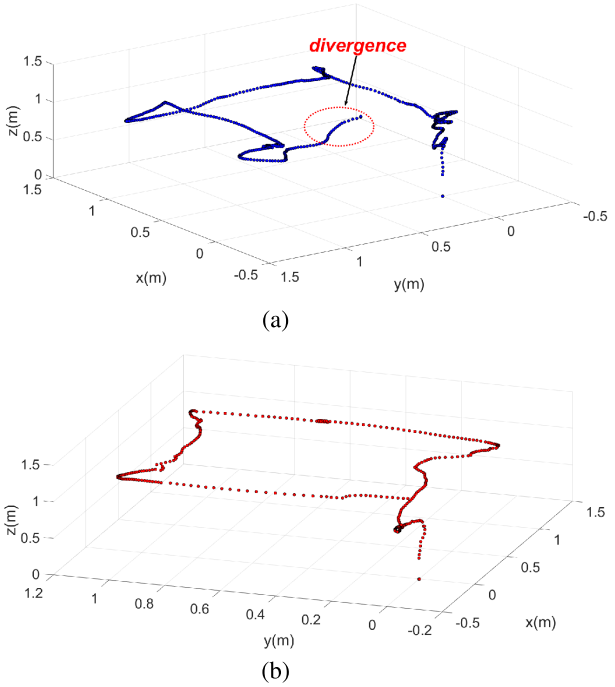

FIGURE 5. Rectangular motion experiment results in 3-dimensional coordinate system: (a) LQG control and (b) FMOFC (proposed).

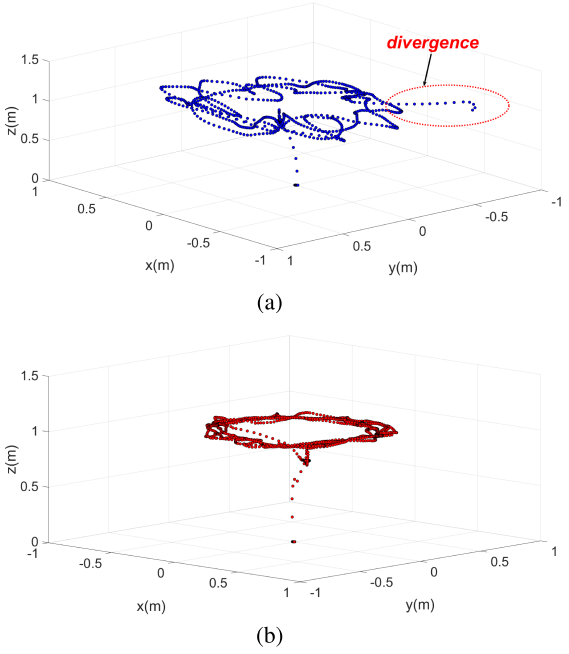

FIGURE 6. Circular motion experiment results in 3-dimensional coordinate system: (a) LQG control and (b) FMOFC (proposed).

hand, the proposed method returned to the given position with smaller amounts of overshoot occurring when the amplitude of the injected disturbance signals and reached only approximately 1.2 meters. The results can be more clearly seen in Table 2, the RMSE comparison table in terms of the x and y positions. As shown in Table 2, the RMSE value of the proposed control strategy was approximately seven and five times lower than the LQG control strategy in the x and y positions, respectively. As a result, the FMOFC shows a robust performance even in the presence of disturbance.

TABLE 2. RMSE comparison in rectangular motion experiment.

	LQG control	FMOFC (proposed)
x position	0.5942	0.0817
y position	0.5563	0.1046

4) CIRCULAR MOTION EXPERIMENT

In the circular motion experiment, the reference values were set to move the drone in the shape of a circle with a radius of 0.5 meters while maintaining a height of 1 meter. A sine curve with an amplitude of 0.1 meters and an impulse with a value of 0.1 meters were injected as disturbance signals during the entire experiment.

The experimental results of the UAV are indicated in a three-dimensional coordinate system, as shown in Fig. 6: (a) LQG control and (b) the proposed method, FMOFC. As shown in Fig. 6(a), initially, the UAV with LQG control maintained a circular path, but significant amounts of overshoot occured in the case of disturbance. However, in the end, the given path was not maintained and the LQG control shows a divergence phenomenon due to the accumulation of errors and the unexpected disturbance. On the other hand, the proposed method maintained the given path even in the presence of disturbance with only small amounts of overshoot as shown in Fig. 6(b). The results can be more clearly seen in Table 3, the RMSE comparison table in terms of the x and y positions. As shown in Table 3, the RMSE value of the proposed control strategy was approximately 11 times lower than the LQG control strategy in the x and y positions. As a result, the FMOFC shows a robust performance against the disturbance.

TABLE 3. RMSE comparison in circular motion experiment.

	LQG control	FMOFC (proposed)
x position	0.6720	0.0612
y position	0.5986	0.0521

IV. CONCLUSION

In this paper, a novel control strategy, FMOFC, for UAV is proposed considering only four independent states (i.e., the x, y, and z velocities in the vehicle coordinate system and yaw rate). The proposed control strategy was designed with the estimated states composed of the velocities in the vehicle coordinate system and the yaw rate from the proposed control law that minimizes the weighted sum of error terms. The controller gain was determined to stabilize the reconstructed dynamical system model in respect of the error

terms. Furthermore, the control inputs to the UAV were derived by obtaining auxiliary control inputs for the reconstructed dynamical system model. The estimated states used for the FMOFC were obtained from the finite memory estimator with the augmented form of four independent states under constraints: the unbiased condition and finite memory structure. Through the definition of the horizon size and augmented horizon size, the FMOFC was derived with the property that the corresponding horizon size for each state could be different and exhibited a finite memory structure. From the final structure of the finite memory estimator with the augmented state, parallel relationships among independent states were demonstrated. The fast convergence and robust performance of the FMOFC under unexpected disturbance were demonstrated through the experimental results: hovering, rectangular motion, and circular motion experiments. Therefore, the FMOFC is considered to be an appropriate control strategy for UAVs in harsh environments such as unexpected disturbance. The proposed control strategy is expected to be applied to various plants and situations, such as formation and flocking systems, by extending the augmented horizon size and augmented state concept to the networked systems or nodes based on the graph theory. Moreover, the FMOFC is expected to guarantee stability and safety through future studies regardless of harsh environments, including uncertainties and couplings.

REFERENCES

[1] P. Tokekar, J. V. Hook, D. Mulla, and V. Isler, "Sensor planning for a symbiotic UAV and UGV system for precision agriculture," *IEEE Trans. Robot.*, vol. 32, no. 6, pp. 1498–1511, Dec. 2016.
[2] M. Haris, T. Watanabe, L. Fan, M. R. Widyanto, and H. Nobuhara, "Super-resolution for UAV images via adaptive multiple sparse representation and its application to 3-D reconstruction," *IEEE Trans. Geosci. Remote Sens.*, vol. 55, no. 7, pp. 4047–4058, Jul. 2017.
[3] L. Lin and M. A. Goodrich, "Hierarchical heuristic search using a Gaussian mixture model for UAV coverage planning," *IEEE Trans. Cybern.*, vol. 44, no. 12, pp. 2532–2544, Dec. 2014.
[4] D. Erdos, A. Erdos, and S. E. Watkins, "An experimental UAV system for search and rescue challenge," *IEEE Aerosp. Electron. Syst. Mag.*, vol. 28, no. 5, pp. 32–37, May 2013.
[5] Y. Lu, D. Macias, Z. S. Dean, N. R. Kreger, and P. K. Wong, "A UAV-mounted whole cell biosensor system for environmental monitoring applications," *IEEE Trans. Nanobiosci.*, vol. 14, no. 8, pp. 811–817, Dec. 2015.
[6] Y. Liu, Q. Wang, Y. Zhuang, and H. Hu, "A novel trail detection and scene understanding framework for a quadrotor UAV with monocular vision," *IEEE Sensors J.*, vol. 65, no. 3, pp. 6778–6787, Oct. 2017.
[7] Y. Yin, X. Wang, D. Xu, F. Liu, Y. Wang, and W. Wu, "Robust visual detection–learning–tracking framework for autonomous aerial refueling of UAVs," *IEEE Trans. Instrum. Meas.*, vol. 65, no. 3, pp. 510–521, Mar. 2016.
[8] T. Oliveira, A. P. Aguiar, and P. Encarnacao, "Moving path following for unmanned aerial vehicles with applications to single and multiple target tracking problems," *IEEE Trans. Robot.*, vol. 32, no. 5, pp. 1062–1078, Oct. 2016.
[9] J. Seo, Y. Kim, S. Kim, and A. Tsourdos, "Collision avoidance strategies for unmanned aerial vehicles in formation flight," *IEEE Trans. Aerosp. Electron. Syst.*, vol. 53, no. 6, pp. 2718–2734, Dec. 2017.
[10] L. V. Santana, A. S. Brandao, and M. Sarcinelli-Filho, "Navigation and cooperative control using the AR.Drone quadrotor," *J. Intell. Robot. Syst.*, vol. 84, pp. 327–350, Dec. 2016.
[11] K. Tanaka, T. Ikeda, and H. O. Wang, "Robust stabilization of a class of uncertain nonlinear systems via fuzzy control: Quadratic stabilizability, H^∞ control theory and linear matrix inequalities," *IEEE Trans. Fuzzy Syst.*, vol. 4, no. 1, pp. 1–13, Feb. 1996.
[12] S. Islam, P. X. Liu, and A. E. Saddik, "Robust control of four-rotor unmanned aerial vehicle with disturbance uncertainty," *IEEE Trans. Ind. Electron.*, vol. 62, no. 3, pp. 1563–1571, Mar. 2015.
[13] F. Chen, R. Jiang, K. Zhang, B. Jiang, and G. Tao, "Robust backstepping sliding-mode control and observer-based fault estimation for a quadrotor UAV," *IEEE Trans. Ind. Electron.*, vol. 53, no. 6, pp. 5044–5056, Aug. 2016.
[14] J. Kim, M. S. Kang, and S. Park, "Accurate modeling and robust hovering control for a quad–rotor VTOL aircraft," *J. Intell. Robot. Syst.*, vol. 57, p. 9, Jan. 2010.
[15] Z. Artstein and G. Weiss, "State nullification by memoryless output feedback," *Math. Control, Signals Syst.*, vol. 17, no. 1, pp. 38–56, Feb. 2005.
[16] F. Yacef, H. Boudjedir, H. Khebbache, and O. Bouhali, "From PID to state feedback attitude stabilization of a quadrotor UAV," *Int. J. Inf. Technol., Control Automat.*, vol. 2, no. 3, pp. 1–13, 2012.
[17] A. Samir, A. Hammad, A. Hafez, and H. Mansour, "Quadcopter trajectory tracking control using state-feedback control with integral action," *Int. J. Comput. Appl., Control Automat.*, vol. 168, no. 9, pp. 1–7, Jun. 2017.
[18] S. Islam, P. X. Liu, and A. E. Saddik, "Observer-based adaptive output feedback control for miniature aerial vehicle," *IEEE Trans. Ind. Electron.*, vol. 65, no. 1, pp. 470–477, Jan. 2018.
[19] M. Tognon, S. S. Dash, and A. Franchi, "Observer-based control of position and tension for an aerial robot tethered to a moving platform," *IEEE Robot. Autom. Lett.*, vol. 1, no. 2, pp. 732–737, Jul. 2016.
[20] A. Dharmawan, A. Ashari, and A. E. Putra, "Translation movement stability control of quad tiltrotor using LQR and LQG," *Int. J. Intell. Syst. Appl.*, vol. 10, no. 3, pp. 10–21, Mar. 2018.
[21] Y.-L. Wang and Q.-L. Han, "Network-based modelling and dynamic output feedback control for unmanned marine vehicles in network environments," *Automatica*, vol. 91, pp. 43–53, May 2018.
[22] X. Dong and G. Hu, "Time-varying output formation for linear multiagent systems via dynamic output feedback control," *IEEE Trans. Control Netw. Syst.*, vol. 4, no. 2, pp. 236–245, Jun. 2017.
[23] T. Tanaka, P. M. Esfahani, and S. K. Mitter, "LQG control with minimum directed information: Semidefinite programming approach," *IEEE Trans. Autom. Control*, vol. 63, no. 1, pp. 37–52, Jan. 2018.
[24] K. Benkhoud and S. Bouallegue, "Dynamics modeling and advanced metaheuristics based LQG controller design for a quad tilt wing UAV," *Int. J. Dyn. Control*, vol. 6, no. 2, pp. 630–651, Jun. 2018.
[25] H.-I. Lee *et al.*, "Parameter-robust linear quadratic Gaussian technique for multi-agent slung load transportation," *Aerosp. Sci. Technol.*, vol. 71, pp. 119–127, Dec. 2017.
[26] L. V. Santana, A. S. Brandao, and M. S. Filho, "On iterative closed-loop identification using affine Takagi–Sugeno models and controllers," *J. Intell. Robot. Syst.*, vol. 8, nos. 1–4, pp. 327–350, Feb. 2016.
[27] A. Schrodt and A. Kroll, "On iterative closed-loop identification using affine Takagi–Sugeno models and controllers," *Int. J. Fuzzy Syst.*, vol. 19, no. 6, pp. 1978–1988, Dec. 2017.
[28] C. Li and M. Z. Q. Chen, "Simultaneous identification and stabilization of nonlinearly parameterized discrete-time systems by nonlinear least squares algorithm," *IEEE Trans. Autom. Control*, vol. 61, no. 7, pp. 1810–1823, Jul. 2016.
[29] M. Z. Q. Chen, L. Zhang, H. Su, and G. Chen, "Stabilizing solution and parameter dependence of modified algebraic Riccati equation with application to discrete-time network synchronization," *IEEE Trans. Autom. Control*, vol. 61, no. 1, pp. 228–233, Jan. 2016.
[30] T. Nguyen and Z. Gajic, "Solving the matrix differential Riccati equation: A Lyapunov equation approach," *IEEE Trans. Autom. Control*, vol. 55, no. 1, pp. 191–194, Jan. 2010.

HYUN HO KANG received the B.S. degree in electrical engineering from Korea University, Seoul, South Korea, in 2017. Since 2017, he has been a Graduate Student with the School of Electrical Engineering, Korea University. His research interests include optimal, robust, and intelligent controls with finite memory structure for unmanned aerial vehicles and multi-agent systems.

SANG SU LEE received the B.S. degree in electrical engineering from Korea University, Seoul, South Korea, in 2017. Since 2017, he has been a Graduate Student with the School of Electrical Engineering, Korea University. His research interests include intelligent, robust, and receding horizon controls for multi-agent systems and system identification for nonlinear systems.

SUNG HYUN YOU received the B.S. degree in electrical engineering from the Seoul National University of Science and Technology, Seoul, in 2013. Since 2013, he has been a Graduate Student with the School of Electrical Engineering, Korea University, Seoul. His research interests include optimal, robust, intelligent, and receding horizon controls.

CHOON KI AHN (M'06–SM'12) received the B.S. and M.S. degrees from the School of Electrical Engineering, Korea University, Seoul, South Korea, in 2000 and 2002, respectively, and the Ph.D. degree from the School of Electrical Engineering and Computer Science, Seoul National University, Seoul, in 2006. He was a Senior Research Engineer with Samsung Electronics, Suwon, South Korea, a Professor with the Department of Mechanical and Automotive Engineering, Seoul National University of Science and Technology, Seoul. He is currently a Crimson Professor of Excellence with the College of Engineering and a Professor with the School of Electrical Engineering, Korea University. He was a recipient of the Early Career Research Award and the Excellent Research Achievement Award of Korea University in 2015 and 2016, respectively.

Dr. Ahn received the Medal for Top 100 Engineers 2010 by IBC, Cambridge, England. In 2012, his EPJE paper was ranked 1 in the TOP 20 Articles in the field of neural networks by BioMedLib. In 2013, his two papers were selected as 5 Key Papers and 5 Popular Papers in *Nonlinear Dynamics* (Springer). In 2015, his paper was ranked 6 in the Top 50 Most Popular Articles for the IEEE TRANSACTIONS ON AUTOMATIC CONTROL. In 2016, he was ranked 1 in electrical/electronic engineering and ranked 2 in entire areas of engineering among korean young professors based on paper quality. In 2017, his two papers were ranked in Most Cited Articles published in the last five years for the IEEE TRANSACTIONS ON CIRCUITS AND SYSTEMS II. In 2017, he received the Presidential Young Scientist Award of Korea.

His current research interests are control, filtering, 2-D system theory, fuzzy systems, neural networks, and nonlinear dynamics. He has been on the Editorial Board of leading international journals, including the *IEEE Systems, Man, and Cybernetics Magazine*, the IEEE TRANSACTIONS ON SYSTEMS, MAN, AND CYBERNETICS: SYSTEMS, the IEEE SYSTEMS JOURNAL, the IEEE/CAA JOURNAL OF AUTOMATICA SINICA, the IEEE ACCESS, *IET Circuits, Devices & Systems*, *Nonlinear Dynamics*, *Aerospace Science and Technology*, *Multidimensional Systems and Signal Processing*, the *International Journal of Systems Science*, the *Journal of The Franklin Institute*, the *International Journal of Circuit Theory and Applications*, *Artificial Intelligence Review*, *Knowledge and Information Systems*, *Neurocomputing*; *Neural Computing and Applications*, the *International Journal of Fuzzy Systems*, and the *International Journal of Machine Learning and Cybernetics*.